Comparison of DODCI fluorescence depolarization in glycerol and ethylene glycol: Effect of orientational correlation on excitation transport

Philip A. Anfinrud and Walter S. Struve

Citation: The Journal of Chemical Physics **87**, 4256 (1987); doi: 10.1063/1.452883
View online: http://dx.doi.org/10.1063/1.452883
View Table of Contents: http://scitation.aip.org/content/aip/journal/jcp/87/8?ver=pdfcov
Published by the AIP Publishing

Comparison of DODCI fluorescence depolarization in glycerol and ethylene glycol: Effect of orientational correlation on excitation transport

Philip A. Anfinrud and Walter S. Struve
Department of Chemistry and Ames Laboratory–USDOE Iowa State University, Ames, Iowa 50011

(Received 19 June 1987; accepted 16 July 1987)

Time-correlated single-photon counting was used to obtain anisotropic fluorescence profiles for DODCI in ethylene glycol. Rotational diffusion of DODCI in this solvent was characterized at a concentration of $\sim 10^{-6}$ M, where minimal electronic excitation transport occurs during the dye fluorescence lifetime. The fluorescence depolarization due to excitation transport at higher concentrations was separated from that due to rotational diffusion; analysis of our data yields excellent agreement with current transport theories. The discrepancies observed between these theories and our earlier DODCI experiments in glycerol [J. Chem. Phys. **86**, 2689 (1987)] appear to originate from orientational correlation of neighboring chromophores in that solvent; glycerol exhibits remarkable coherence in its total radial distribution function out to separations as large as 25 Å at temperatures between 250 and 350 K [Z. Naturforsch. Teil A **36**, 1045 (1981)].

I. INTRODUCTION

Our laboratory has recently been assessing fluorescence concentration depolarization techniques as a means of testing electronic excitation transport theories for molecules in disordered systems.[1–3] Fluorescence depolarization measurements are not an inherently sensitive probe of transport, even in systems of randomly oriented molecules.[2] Polarized fluorescence profiles with $S/N > 10^2$ are typically required for meaningful tests of transport theories; small artifacts can easily invalidate such work. In our first study of excitation transport in solution,[1] we exploited time-correlated photon counting to monitor fluorescence depolarization from rhodamine 6G at concentrations between 0.17 and 2.4 mM in glycerol. It was shown that artifacts arising from excitation trapping by dye aggregates and from fluorescence self-absorption[4] readily dominate the residuals between experimental fluorescence profiles and profiles calculated from current transport theories, such as the Gochanour–Andersen–Fayer (GAF) self-consistent three-body theory.[5] These artifacts were minimized in subsequent experiments on DODCI in glycerol,[2] by housing sample solutions in fluorescence cells $\lesssim 2\,\mu$m thick and by maintaining dye concentrations below ~ 3 mM to inhibit dye aggregation. Some 10^5 photon counts were typically accumulated in the peak channel of DODCI fluorescence profiles, as compared to $\sim 10^4$ counts in the rhodamine 6G experiments. Under these conditions, a still smaller artifact became discernible[2] during the first ~ 200 ps of each profile. Its origin was confirmed to be solvent reorganization, which originated from a disparity in dipole moments between the dye S_0 and S_1 electronic states and caused dynamic shifting of the DODCI fluorescence spectrum at early times. (DODCI profiles were monitored for ~ 9 ns, corresponding to $\sim 5.3\,S_1$ state lifetimes in glycerol.) The algebraic sign of this early-time artifact could be manipulated by using optical filters to concentrate our spectral sensitivity to the red or to the blue of the peak in the DODCI static fluorescence spectrum. In the former case, the dynamic Stokes shift contributed a short component with negative preexponential factor to the isotropic fluorescence decay. In the latter case, the preexponential sign was positive, because the overlap between the dynamic fluorescence spectrum with our spectral sensitivity decreased at early times. Nonlinear least-squares fitting of our time-resolved profiles with model functions based on transport theories yielded similar optimized parameters for either combination of filters. In this manner, the solvent reorganization artifact was demonstrated to have little effect on multiparameter fitting of transport theories to our polarized fluorescence profiles.

For all of these precautions, the discrepancies observed between our DODCI profiles[2] and current transport theories[5–7] remained physically large. When randomly oriented, nonrotating molecules in three dimensions are excited by a weak, linearly polarized laser pulse, the emitted fluorescence components $I_{\|}(t)$ and $I_{\perp}(t)$ polarized parallel and normal to the excitation polarization are approximately related to the probability $G^s(t)$ that the excitation is found on the initially excited molecule by

$$I_{\|}(t) = P(t)\,[1 + 0.8G^s(t)],$$
$$I_{\perp}(t) = P(t)\,[1 - 0.4G^s(t)]. \quad (1)$$

Here $P(t)$ is the isotropic decay function, which is theoretically single-exponential for a sufficiently dilute, homogeneous dye solution. [$P(t)$ was represented by biexponential functions in our earlier DODCI work to account for the solvent reorganization artifact.[2]] The Green's function $G^s(t)$ was modeled by either the GAF three-body theory[5] [which yields a complicated but analytic[6] expression for $G^s(t)$] or the two-particle theory of Huber *et al.*[7] The latter theory predicts that at sufficiently early times and/or low dye concentrations,

$$G^s(t) = \exp\left[-C\left(\frac{\pi t}{2\tau}\right)^{1/2}\right]. \quad (2)$$

Both of these theories contain as parameters the intrinsic excited state lifetime τ and the dimensionless reduced dye concentration

 0021-9606/87/204256-07$02.10

$$C = \tfrac{4}{3}\pi R_0^3 \rho, \tag{3}$$

where ρ is the molecule number density and R_0 is the Förster parameter.[8] The GAF three-body and Huber two-particle theories yield nearly identical decay functions $G^s(t)$ for $C = 1.0$ and $t \lesssim 5\tau$,[2] so that these two theories are virtually indistinguishable for realizable dye concentrations in glycerol and for measurable time windows. The discrepancies between our polarized DODCI profiles and the Huber two-particle theory are summarized in Fig. 1, which was generated by fitting data taken from Ref. 2. Here the optimized reduced concentration C [obtained by fitting profiles with Eqs. (1), using either GAF three-body or Huber theory for $G^s(t)$] are plotted vs the actual dye concentration. For a perfect theory, the points in Fig. 1 should fall on a straight line of constant R_0. Since these points skew systematically from $R_0 \sim 63$ Å to $R_0 \sim 53$ Å as M is increased from ~ 0.2 to 1.8 mM, the apparent strength of the dipole–dipole coupling (which scales as $R_0^{6.8}$) artificially increases by a factor of ~ 2.8. [Detection of even such a large discrepancy required fluorescence profiles with peak S/N ~ 300 ($= \sqrt{10^5}$)]. We were unable to explain this disagreement.

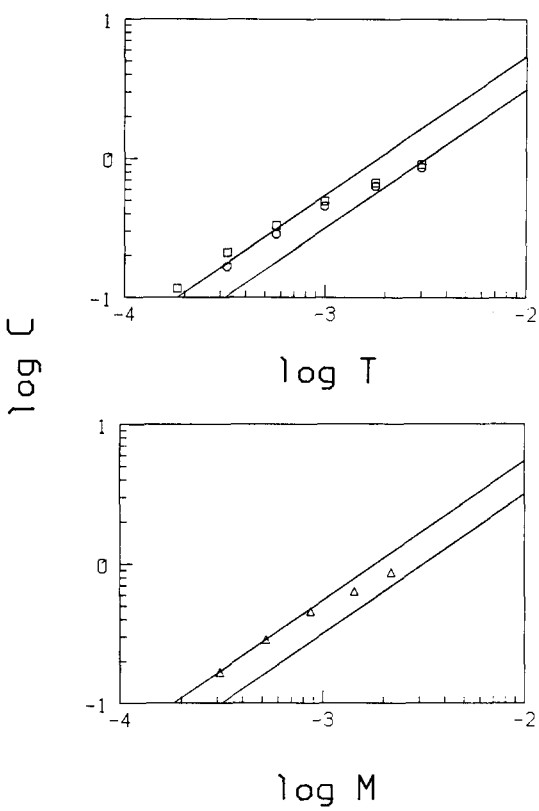

FIG. 1. (a) Optimized reduced concentrations C_D vs total DODCI concentrations $[T]$ in glycerol, from linked deconvolution of $I_\parallel$ and $I_\perp$ fluorescence profiles (Ref. 2) using Eqs. (1). The GAF three-body and the Huber two-particle theories for $G^s(t)$ yield similar results. Straight lines give loci of true reduced concentrations vs monomer concentrations $[M]$ for (from left) $R_0 = 60$, 50 Å. Points labeled (○) and (□) were obtained from data analyses considering and neglecting rotational depolarization, respectively. (b) A plot generated from the same data set as in (a), but analyzed taking both rotational depolarization and dimerization equilibrium into account. Horizontal axis is DODCI monomer concentration $[M]$; straight lines correspond to (from left) $R_0 = 60$, 50 Å.

Since the publication of this work, several possible sources have been considered for the discrepancy. The use of Eqs. (1) to analyze fluorescence data rests on the assumption that the residual polarization

$$P_1 = (I_\parallel - I_\perp)/(I_\parallel + I_\perp) \tag{4}$$

retained in an orientationally random solution after a single excitation hop from the initially excited molecule is zero. Galanin has shown that $P_1 = 1/42$ in a random three-dimensional system.[9] We have reanalyzed our DODCI data accordingly,[10] and have shown that consideration of this residual polarization barely affects the discrepancy in Fig. 1.

While rotational diffusion of DODCI in glycerol is slow compared to the intrinsic S_1 state decay, it does contribute slightly to the total fluorescence depolarization during our 9 ns time window. This rotational depolarization can be independently characterized in very dilute solution ($\sim 10^{-6}$ M), where excitation transport is negligle. The rotational diffusion component of the total fluorescence depolarization proves to be separable from the excitation transport component, so that transport theories can be tested even in the presence of rotational diffusion. Using an analysis described in Sec. III, we find that the rotational depolarization of DODCI in glycerol is well described by a single-exponential anisotropy function with lifetime $\tau_{rot} = 69$ ns. When the corresponding contribution to the fluorescence depolarization is separated from the transport component, fitting the latter with the Huber two-particle theory yields results which are contrasted with the results obtained neglecting rotational diffusion in Fig. 1(a). While failure to consider rotational diffusion affects all of the data points (particularly at the lower concentrations where transport depolarization is minor), the discrepancy remains large.

A third source of error arises because not all DODCI species exist as monomers in glycerol. The abscissa in Fig. 1(a), putatively the dye monomer concentration $[M]$, is actually the total dye concentration $[T] \simeq [M] + 2[M_2]$. Equating $[M]$ with $[T]$ will skew the data points downward at higher concentrations, because the ratio $[M_2]/[M]$ will increase with $[T]$. We evaluated the dimerization equilibrium constant $K_d = [M_2]/[M]^2$ by obtaining DODCI absorption spectra at several concentrations in glycerol, and by measuring optical densities at the M and M_2 band maxima at 575 and 545 nm, respectively. The inferred K_d depends on the values assumed for the absorption coefficients ϵ_{max} (M) and ϵ_{max} (M_2). A dilute DODCI spectrum yielded the former; the latter is bounded by ϵ_{max} $(M) \leqslant \epsilon_{max}$ (M_2) $\leqslant 2\epsilon_{max}$ (M), depending on the vector addition of monomer transition moments in the dimer.[11] In the worst case [ϵ_{max} $(M) = \epsilon_{max}$ (M_2)], it is found that some 27% of DODCI molecules exist in dimers in glycerol when $[T]$ = 3.0 mM. When both rotational depolarization and dimerization are taken into account (assuming ϵ_{max} is identical for both M and M_2), the modified plot in Fig. 1(b) results. The data skewing is now significantly reduced, but it is still large.

Yet another possible origin for the discrepancy is nonrandomness in molecular orientations. Since the average separation between DODCI pairs is on the order of 30 Å in our most concentrated solutions, such nonrandomness

would have to be a consequence of long-range ordering in the solvent structure. Such ordering is absent in most alcohols at room temperature (Sec. IV). Glycerol has been used in previous fluorescence experiments on solution transport,[1,2,12] because its large viscosity (954 cp at 25 °C[13]) precludes large contributions to depolarization from rotational diffusion. In liquid glycerol, however, the radial distribution functions derived from x-ray structure factors obtained between 250 and 350 K exhibit coherent oscillations out to separations larger than 25 Å.[14] Hence, sufficiently concentrated DODCI solutions in glycerol are likely to exhibit appreciable orientational correlation between neighboring chromophores. If DODCI neighbors tend to have parallel transition moments, for example, a single excitation hop will produce less depolarization than in an orientationally random sample. The residual polarization P_1 will then become appreciable, rendering Eqs. (1) inapplicable. The nonrandom orientational distributions would also influence the calculation of $G^s(t)$. The significance of this effect would increase with dye concentration, as the solvent ordering asserts itself at shorter chromophore separations.

In this work, we have obtained polarized fluorescence profiles for DODCI in ethylene glycol, a solvent which does not exhibit comparable long-range ordering at room temperature (Sec. IV). The bulk viscosity of ethylene glycol (17.4 cp at 25 °C[13]) is some two orders of magnitude smaller than that of glycerol, and rotational diffusion of DODCI in ethylene glycol contributes substantially to the total fluorescence depolarization observed in that solvent. DODCI dimerization is much less prevalent in ethylene glycol than in glycerol, however. When our DODCI profiles from glycol solutions are analyzed with due attention to rotational depolarization and the dimerization equilibrium, close agreement is obtained with the Huber and GAF three-body theories (Sec. IV). This result strongly suggests that orientational correlation accounts for most of the unexplained discrepancy exhibited by DODCI/glycerol in Fig. 1(b).

II. EXPERIMENTAL SECTION

The tunable picosecond excitation laser system,[1] composed of a mode-locked argon ion laser, synchronously pumped rhodamine 590 laser, and cavity dumper, generated 570 nm pulses with ~7 ps FWHM at 4.8 MHz repetition rate. DODCI (3,3'-diethyloxadicarbocyanine iodide) was supplied by Exciton; purified ethylene glycol was obtained from Fisher Scientific, and contributed no background counts to fluorescence profiles from DODCI solutions. DODCI emission was analyzed with a Promaster Spectrum 7 linear polarizer, passed through two 3 mm Schott OG-590 filters, collected with a 10 cm f.l. quartz lens, and focused through a variable rectangular aperture onto a Hamamatsu R1564U microchannel plate phototube (MCP). The time-correlated photon counting electronics[2] included a B&H Electronics AC3011 MIC 3.15 GHz preamplifier, a Tennelec TC455 constant-fraction discriminator (CFD), and an Ortec 457 time-to-amplitude converter (TAC). One channel of the TC455 CFD was modified to accept positive-going pulses from the preamplifier, and generated the START input for the TAC. The STOP input was provided by a second TC455 channel which processed negative-going pulses from an EG&G FOD-100 laser-monitoring photodiode. Crosstalk between the channels (which caused TAC nonlinearity) was eliminated by delaying the photodiode signal relative to the MCP signal in a 15 m fiber optic. Fluorescence profiles were accumulated in a Canberra Series 30 multichannel analyzer with 20 ps/channel resolution. The TAC was automatically gated off by a 125 μs gating pulse derived from the TAC's true START output, effectively eliminating count-rate dependence in time-to-amplitude conversion while allowing count rates up to ~8 kHz.[2] Fluorescence profiles were obtained at ~5 kHz count rate; instrument functions (evaluated by detecting 570 nm laser pulses scattered from a roughened fused silica substrate in place of the sample housing) were ~47 ps FWHM.

Polarized DODCI fluorescence profiles were obtained using ethylene glycol solutions in specially designed optical cells with $\lesssim 2$ μm path length to minimize self-absorption.[2] For excitation transport studies, the DODCI concentrations ranged between 0.315 and 5.61 mM. In separate calibration runs, the rotational diffusion of DODCI in ethylene glycol was studied by obtaining polarized profiles from 0.98 μM solutions; 100 μm cells were used here without danger of incurring self-absorption artifacts. At the latter concentration, the decay in $G^s(t)$ due to transport is negligible during our ~9 ns time window. The ambient temperature during both sets of runs was 23.5 °C.

III. DATA ANALYSIS

Fluorescence profiles were accumulated for each DODCI sample with the analyzing polarizer aligned at $\theta = 0°$, 54.7°, and 90° from the laser polarization in order to obtain the experimental $I_{\parallel}(t)$, magic-angle, and $I_{\perp}(t)$ profiles, respectively. The isotropic decay function $P(t)$ from the magic-angle profile at each concentration was fitted with a biexponential decay law using a Marquardt nonlinear least-squares program,[15] with the results shown in Table I. The isotropic decay is dominated in all cases by a long component with lifetime $\tau_1 \sim 1.2$ ns in ethylene glycol (vs 1.7 ns in glycerol[2]). This lifetime is nearly constant for concentrations up to 1.78 mM, and shows no stretching due to self-absorption. At the highest two concentrations (3.14 and 5.61 mM) τ_1 drops to 1.151 and 1.022 ns, respectively, due to excitation trapping at aggregates. The small short component τ_2 (436 to 563 ps) arises chiefly from the solvent reorganization artifact[2] at the lower concentrations, but may also

TABLE I. Magic-angle fits of DODCI fluorescence profiles in ethylene glycol. $P(t) = a_1 \exp(-t/\tau_1) + a_2 \exp(-t/\tau_2)$.

Concentration, mM	a_1	τ_1, ps	a_2	τ_2, ps	χ_r^2
0.000 98	0.903	1297	0.097	563	1.256
0.315	0.898	1284	0.102	509	1.092
0.558	0.908	1271	0.092	436	1.222
0.988	0.905	1260	0.095	458	0.959
1.78	0.870	1237	0.130	508	1.067
3.14	0.838	1151	0.162	483	1.210
5.61	0.617	1022	0.383	504	1.430

be influenced by excitation trapping at 3.14 and 5.61 mM. Good single-exponential fits to isotropic profiles are frequently reported for dyes in dilute alcohol solutions, probably because the nonexponentiality from the dynamic Stokes shift is obscured by noise in profiles with less favorable counting statistics. In the course of this work, it became recognized that the commonly used technique for calculating the discrete convolution

$$F(I)=\sum_{J=0}^{I} X(J)D(I-J) \tag{5}$$

of the apparatus instrument function $X(J)$ with the fitted decay law $D(I)$ is not strictly accurate. Since $X(J)$ is a histogram (rather than continuous) representation of the instrument function, the convolution procedure requires that the discrete function $D(I)$ be a histogram representation

$$D(I)\equiv\int_{I-1/2}^{I+1/2} D(x)dx \tag{6}$$

of the continuous function $D(x)$ instead of

$$D(I)=D(x)|_{x=I}. \tag{7}$$

In fitting with the single-exponential decay law $D(x)=a\exp(-x/\gamma)$, for example, the discrete decay law should be

$$\begin{aligned} D(I)&=a\int_{I-1/2}^{I+1/2}\exp(-x/\gamma)dx \\ &=a\gamma\{\exp[-(I-1/2)/\gamma] \\ &\quad-\exp[-(I+1/2)/\gamma]\}, \end{aligned} \tag{8a}$$

$$D(0)=a\gamma\{1-\exp[-1/2\gamma]\}, \tag{8b}$$

instead of $D(I)=a\exp(-I/\gamma)$. For decay models which cannot be integrated analytically, Simpson's rule is used to generate the histogram representation of $D(I)$. The numerical differences between this and earlier[1–3] calculations of the discrete convolution assume importance when $D(x)$ changes rapidly during a single channel (20 ps in our work). Hence, the associated errors are concentrated in the peak regions at early times, and they primarily affect the short-component parameters in Table I. They do not materially influence the conclusions reached in earlier work,[1–3] where the fitted excitation transport parameters largely depended on fluorescence depolarization evolving over several ns.

The polarized fluorescence profiles obtained at 0.98 μM (the limit of zero excitation transport) were then fitted with the decay laws

$$\begin{aligned} I_{\parallel}(t)&=aP(t)[1+0.8e^{-6Dt}], \\ I_{\perp}(t)&=a_{\perp}P(t)[1-0.4e^{-6Dt}]. \end{aligned} \tag{9}$$

These expressions are applicable to rotational diffusion of a spherical rotor with angle $\lambda=0°$ between absorption and fluorescence transition moments.[16] The DODCI transition moment lies essentially parallel to the long axis; earlier attempts to fit polarized DODCI profiles in glycerol by floating λ as a parameter[2] tended to force λ toward 0°. Rotational diffusion of an asymmetric rotor in three dimensions is characterized by five time constants in general.[16] However, DODCI rotation about the long axis is expected to cause negligible depolarization. The other two rotation axes in this highly prolate molecule will exhibit similar diffusion constants, which are represented by D in Eqs. (9). In fitting these equations to the low-concentration anisotropic profiles, the isotropic decay $P(t)$ was simulated by a biexponential function with fixed parameters taken from the first line of Table I. As in earlier work,[1,2] $I_{\parallel}(t)$ and $I_{\perp}(t)$ were fitted simultaneously by optimizing their combined χ_r^2. The only parameters varied were the scaling factors $a_{\parallel}$, $a_{\perp}$ and the diffusion constant $D\equiv 1/6\tau_{\rm rot}$; their final values are given in Table II. This linked deconvolution of $I_{\parallel}$ and $I_{\perp}$ yields the single reorientation time $\tau_{\rm rot}=3.22$ ns; the relative qualities of fits are reflected by the values of χ_r^2 calculated separately for each profile following optimization of their combined χ_r^2. In Fig. 2, the experimental isotropic and anisotropic profiles of 0.98 μM DODCI are compared with their fitted model functions. The isotropic profile $P(t)$ is clearly well described by a biexponential decay law, and the pertinent autocorrela-

TABLE II. Results of linked deconvolution of 0.98 μM anisotropic DODCI profiles in ethylene glycol. $I_{\parallel}(t)=a_{\parallel}P(t)[1+0.8\exp(-6Dt)]$; $I_{\perp}(t)=a_{\perp}P(t)[1-0.4\exp(-6Dt)]$.

Profile	$\tau_{\rm rot}$, ns	χ_r^2
$I_{\parallel}(t)$	3.223	1.891
$I_{\perp}(t)$	3.223	1.225

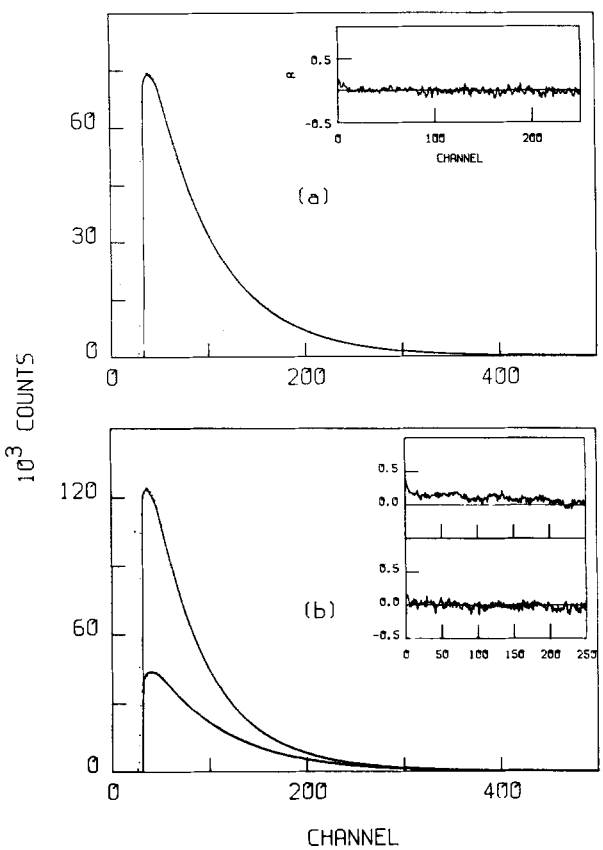

FIG. 2. (a) Isotropic fluorescence profile and (b) anisotropic fluorescence profiles of 0.98 μM DODCI in ethylene glycol. Inset plots show autocorrelations of weighted residuals for (from top) $P(t)$, $I_{\parallel}(t)$, and $I_{\perp}(t)$. Time calibration is 20 ps/channel.

tion of residuals[17] is dominated by statistical noise. The anisotropic fits are less good: χ_r^2 is 1.891 for $I_\parallel(t)$, as compared to 1.256 for the isotropic function $P(t)$, and the autocorrelations for these fits exhibit nonstatistical deviations (Fig. 2). We are not aware of other measurements of $\tau_{\rm rot}$ for DODCI in ethylene glycol. Waldeck and Fleming studied rotational diffusion of DODCI in several linear alcohols,[18] and found $\tau_{\rm rot} \sim 1.4$ ns in *n*-decanol. This is lower than the value we obtain in glycol, presumably because *n*-decanol has a smaller viscosity (12 cp at 23 °C). A more detailed orientational diffusion model than the spherical rotor may yield better anisotropic fits; we comment on the effects of these deviations on the interpretation of our transport data in the following section.

In the presence of excitation transport at higher DODCI concentrations, Eqs. (9) for the anisotropic fluorescence intensities become superseded by

$$I_\parallel(t) = a_\parallel P(t)[1 + 0.8\ G^s(t)\exp(-6Dt)],$$
$$I_\perp(t) = a_\perp P(t)[1 - 0.4\ G^s(t)\exp(-6Dt)], \quad (10)$$

if one assumes that the residual polarization P_1 after a single excitation hop is zero. In this limit, all of the polarization stems from excitation residing on the laser-excited molecule. The anisotropic profiles accumulated at DODCI concentrations from 0.315 to 5.61 mM were fitted using Eqs. (10). The isotropic decays $P(t)$ were modeled using biexponential functions with fixed preexponential and lifetime parameters taken from Table I. The reorientation time $\tau_{\rm rot}$ ($= 1/6D$) was maintained at 3.223 ns (Table II). The Huber two-particle function [Eq. (2)] was used for $G^s(t)$; the intrinsic lifetime τ was fixed at 1.300 ns, which closely approximates the long-component lifetime $\tau_1 = 1.297$ ns found in the isotropic decay at 0.98 μM [the low-concentration limit in which trapping artifacts in $P(t)$ are negligible]. Aside from $a_\parallel$ and $a_\perp$, the reduced concentration C in the two-particle approximation to $G^s(t)$ was the only variable parameter in these fits.

IV. RESULTS AND DISCUSSION

The optimized reduced concentrations C and χ_r^2 are listed for the fitted anisotropic profiles in Table III. The two-particle formulation of $G^s(t)$ in Eq. (2) is derived from the orientationally averaged excitation transport rate from molecule *i* to molecule *j*,

$$\frac{dp_i}{dt} = -\frac{1}{\tau}\left(\frac{R_0}{r_{ij}}\right)^6 p_i. \quad (11)$$

When the correct dipole–dipole orientation dependence of dp_i/dt is taken into account, one finds that the reduced concentration C in Eq. (2) must be replaced by γC, with $\gamma = 0.846$.[12] This is reflected in the third column in Table III, which gives the physical reduced concentrations C_D corresponding to the optimized C parameters in our linked deconvolutions of anisotropic profiles. The quality of most fits at the higher concentrations is exemplified by our data for 0.988 mM in Fig. 3. The fluorescence depolarization (evidenced by the rate of coalescence of the $I_\parallel$ and $I_\perp$ profiles) is noticeably more rapid here than at 0.98 μM in Fig. 2, because excitation transport furnishes an additional depolarization mechanism at the higher concentration. As in the 0.98 μM solution (Fig. 2), the isotropic profile $P(t)$ is well approximated by a biexponential decay law. The fit is less impressive for $I_\parallel(t)$, and in fact the nonstatistical autocorrelation of residuals for $I_\parallel(t)$ at 0.988 mM physically resembles that for $I_\parallel(t)$ at 0.000 98 mM, where rotational diffusion dominates the anisotropy (Fig. 2). The autocorrelations at all other concentrations except 5.16 mM [where excitation trapping appreciably distorts $P(t)$, Table I] are similar to those in Figs. 2 and 3. This suggests that at concentrations other than 5.16 mM, the nonstatistical character in the autocorrelation functions originates primarily from the

TABLE III. Results of linked deconvolution of anisotropic DODCI profiles at higher concentrations in ethylene glycol. $I_\parallel(t) = a_\parallel P(t)[1 + 0.8\ G^s(t)\exp(-6Dt)]$; $I_\perp(t) = a_\perp P(t)[1 - 0.4\ G^s(t) \times \exp(-6Dt)]$.

Concentration, mM	C	$C_D = C/\gamma$	$\chi_r^2(\parallel)$	$\chi_r^2(\perp)$
0.315	0.126	0.149	1.465	1.315
0.558	0.225	0.266	1.494	1.178
0.988	0.416	0.491	1.533	1.226
1.78	0.767	0.907	1.736	1.184
3.14	1.43	1.70	1.649	1.584
5.61	2.62	3.09	1.783	2.046

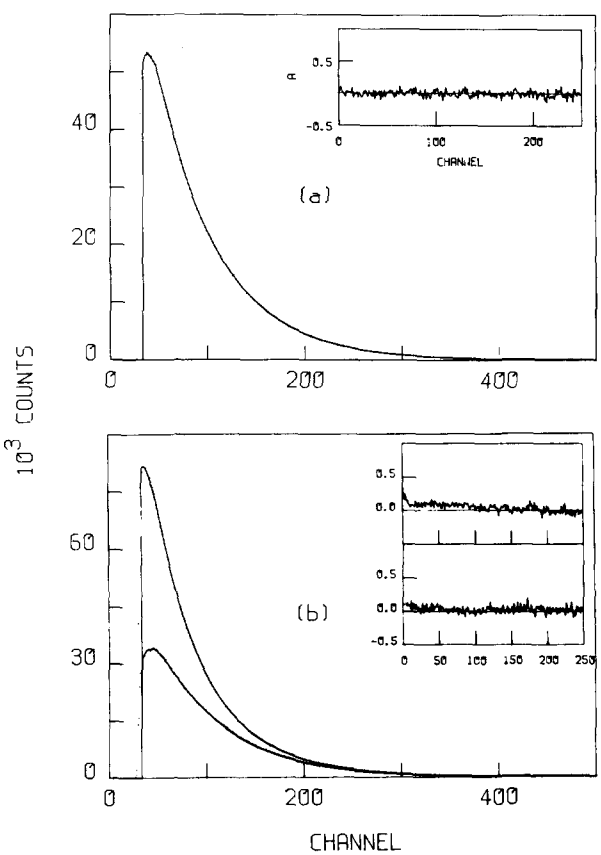

FIG. 3. (a) Isotropic fluorescence profile and (b) anisotropic fluorescence profiles of 0.988 mM DODCI in ethylene glycol. Inset plots show autocorrelations of weighted residuals for (from top) $P(t)$, $I_\parallel(t)$, and $I_\perp(t)$. Time calibration is 20 ps/channel.

spherical rotor approximation in our rotational diffusion model, rather than from problems in our modeling of $G^s(t)$.

In Fig. 4, we plot the optimized reduced concentrations C_D from Table III vs the actual dye monomer concentrations $[M]$. The format of this figure for ethylene glycol is identical to that of Fig. 1 for glycerol. The discrepancies between the experimental points and the theory are clearly far smaller in ethylene glycol than in glycerol. The experimental conditions of the present work were nearly identical to those in our earlier DODCI experiments in glycerol. The slight upward skewing shown in Fig. 4 for ethylene glycol at the higher concentrations may be due to trapping artifacts. A theory which ignores trapping [e.g., Eq. (2)] tends to overestimate $G^s(t)$; the fitting procedure would then yield inflated values of C_D at concentrations where trapping is important. It is interesting that the discrepancies remain small up to 5.61 mM in ethylene glycol (R_0 varies by $\lesssim 2.5$ Å), even though excitation trapping considerably distorts $P(t)$ at this concentration (Table I). Hence, the Huber two-particle theory (and by implication the GAF three-body theory) appears to work well throughout this concentration range in ethylene glycol. This contrasts markedly with the situation in glycerol [Fig. 1(b)].

The microstructure of liquid alcohols has received increased attention in recent years. Monte Carlo simulations of liquid methanol[19] and ethanol[20] indicate that near 25 °C these alcohols consist of irregularly winding chains of sequentially hydrogen-bonded monomers. Distinct peaks attributable to nearest-neighbor and second nearest-neighbor molecular pairs appear in the radial correlation functions generated by such simulations. Like the correlation functions obtained from x-ray analyses of liquid methanol and ethanol,[21] these theoretical functions exhibit little radial correlation beyond separations of 5 to 6 Å. Similar conclusions are obtained using the RISM integral equation approach to simulate methanol.[22] In such solvents, essentially random orientations may be expected for dye molecules separated by tens of Å.

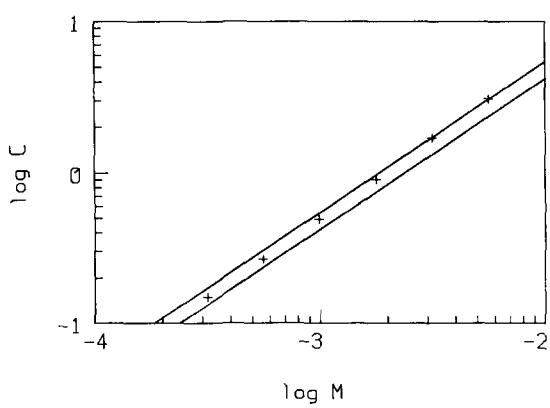

FIG. 4. Optimized reduced concentrations C_D vs actual DODCI monomer concentrations $[M]$ in ethylene glycol, from linked deconvolution of $I_\parallel$ and $I_\perp$ fluorescence profiles using Eqs. (10) (see the text). The Huber two-particle theory is used for $G^s(t)$, and the rotational diffusion parameter is taken from Table II. Straight lines give loci of true reduced concentrations vs $[M]$ for (from left) $R_0 = 60$ and 55 Å.

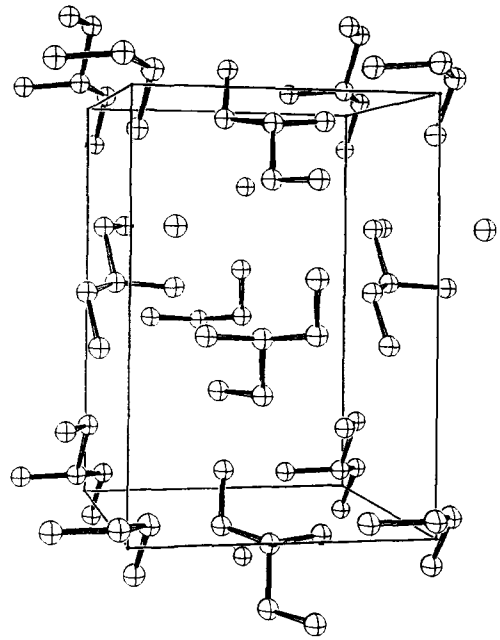

FIG. 5. Crystal structure of orthorhombic glycerol ice, $CH_2OHCHOHCH_2OH$ (calculated from atomic positions and space group symmetry given in Ref. 21). Hydrogen atom positions are not shown. The a and b axes are horizontal and vertical, respectively.

The crystal structure of solid glycerol ($CH_2OHCHOHCH_2OH$) at -75 °C was reported by van Koningsveld.[23] It crystallizes in the orthorhombic space group $P2_12_12_1$ ($Z = 4$) with six hydrogen bonds in a unit cell ($a = 7.00$ Å, $b = 9.96$ Å, $c = 6.29$ Å). As shown in Fig. 5 (plotted using the atomic coordinates reported by van Koningsveld together with the $P2_12_12_1$ equivalent positions), the molecular conformation in solid glycerol is the $\alpha\alpha$-staggered conformation in the Bastiansen nomenclature.[24] This conformation is also found to predominate in liquid glycerol,[14] where the radial correlation function computed from the Fourier-transformed x-ray scattering intensity distribution exhibits strong coherent peaks out to more than 25 Å (several unit cell dimensions). Such long-range solvent ordering is likely to contribute to orientational correlation among nonspherical guest chromophores for nearest-neighbor distances in the tens of Å. The sign of the discrepancies in Fig. 1 is consistent with an increased predominance of parallel neighbors at higher concentrations; no depolarization attends excitation transport in the limit of parallel chromophores, and so the apparent reduced concentration C becomes depressed relative to its true value as the concentration increases. There is little evidence of comparable ordering in the liquid structure of pure ethylene glycol. Several conformations, including intramolecularly hydrogen-bonded molecules of *gauche* geometry as well as *trans* molecules, appear to be important in the liquid.[25,26] There is indirect evidence of two-dimensional structure in ethylene glycol methyl ether.[27] Time-resolved orientational diffusion experiments have demonstrated that tetracene rotates comparatively much more rapidly in its molecular plane in glycol than in 1-dodecanol[28]; this supports the existence of a locally layered microstructure in glycol. Unlike a number of other alcohol ices of low molecular weight (e.g., methanol,

ethanol, glycerol), glycol ice has no entry in the comprehensive NBS-JCPDS Crystal Data compilations as of 1981.[29] We are not aware of any published glycol liquid structure factor determination, despite its important commercial uses in solvents, coolants, and as an intermediate in polymer production. Hence, the long-range radial correlations in liquid glycerol[14] appear to be absent in glycol, and orientational correlation is a likely origin for the contrast in transport behavior between these two solvents.

Quantitative consideration of the orientational correlation required to produce the discrepancies shown in Fig. 1(b) raises interesting questions about the microstructure in glycerol. At the highest concentration used ($\sim$3 mM), the optimized reduced concentration C_D is $\sim$59% of the actual C_D value (computed using $R_0 \sim 64$ Å for DODCI in glycerol[2]) if $\epsilon_{\max}(M) = \epsilon_{\max}(M_2)$. Some 41% of the DODCI chromophores are thus presumably hidden by orientational correlation at this concentration when transport is monitored by fluorescence depolarization. The differential probability that a nearest neighbor resides at separation R from a given DODCI molecule in a spatially random distribution is[30]

$$dP(R) = 4\pi R^2 \rho \exp(-4\pi R^3 \rho/3) dR, \tag{12}$$

where ρ is the DODCI number density in the solution. The most probable nearest-neighbor separation is then

$$R_{\mathrm{mp}} = (2\pi\rho)^{-1/3}. \tag{13}$$

At 3 mM, R_{mp} becomes 44 Å. The probability $Q(R)$ that a particular DODCI molecule has a nearest neighbor lying within separation R is

$$Q(R) = \int_0^R P(R')dR' = 1 - \exp(-4\pi R^3 \rho/3). \tag{14}$$

At our highest concentration, 11.2% of the DODCI molecules then have nearest neighbors within $R = 25$ Å if the molecules are randomly distributed. The fraction of the total dipole–dipole excitation transport occurring at distances $\leqslant R$ is

$$f(R) = S(R)/S(\infty), \tag{15}$$

where

$$S(R) = \int_0^R dP(R')/[1 + (R'/R_0)^6] \tag{16}$$

if orientationally averaged transition rates are used. When $f(R)$ is evaluated in this manner, one finds that 15% of the total transport is expected to occur at separations shorter than 25 Å when the concentration is 3 mM. Equation (16) is easily modified to accommodate nonrandom orientational distributions: $f(R)$ may be computed under the crude assumption that all DODCI molecules separated by $R \leqslant R_c$ have mutually parallel transition moments, but have uncorrelated orientations for $R > R_c$. (So defined, R_c represents an orientational "correlation length.") The value of the correlation length R_c which then renders $f(R_c)$ equal to the observed fraction 0.41 of "orientationally hidden" molecules is 39.9 Å. [If $\epsilon_{\max}(M_2)$ is assumed to be $2\epsilon_{\max}(M)$ instead of $\epsilon_{\max}(M)$, R_c becomes 41.9 Å.] This orientational correlation length is appreciably greater than the decay length of $\sim$25 Å shown by the radial correlation function from x-ray scattering in liquid glycerol.[14] Our results therefore suggest that either orientational correlations in liquid glycerol persist to considerably longer separations than radial correlations (as in liquid crystals), or the spatial distribution of DODCI molecules becomes increasingly nonrandom at higher concentrations. Experimental techniques for measurement of orientational correlations in liquids are scarce, and fluorescence concentration depolarization using nonspherical chromophore molecules offers a potentially sensitive probe for this aspect of liquid structure.

ACKNOWLEDGMENTS

The Ames Laboratory is operated for the U.S. Department of Energy by Iowa State University under Contract No. W-7405-Eng-82. This work was supported by the Office of Basic Energy Sciences. We thank Professor Michael Fayer and Professor Robert Jacobson for valuable discussions.

[1] P. A. Anfinrud, D. E. Hart, J. F. Hedstrom, and W. S. Struve, J. Phys. Chem. **90**, 2374 (1986).
[2] D. E. Hart, P. A. Anfinrud, and W. S. Struve, J. Chem. Phys. **86**, 2689 (1987).
[3] P. A. Anfinrud, D. E. Hart, J. F. Hedstrom, and W. S. Struve, J. Phys. Chem. **90**, 3116 (1986).
[4] P. R. Hammond, J. Chem. Phys. **70**, 3884 (1979).
[5] C. R. Gochanour, H. C. Andersen, and M. D. Fayer, J. Chem. Phys. **70**, 4254 (1979).
[6] S. G. Fedorenko and A. I. Burshtein, Chem. Phys. **98**, 341 (1985).
[7] D. L. Huber, D. S. Hamilton, and B. Barnett, Phys. Rev. B **16**, 4642 (1977).
[8] Th. Förster, Discuss. Faraday. Soc. **27**, 7 (1959).
[9] M. D. Galanin, Tr. Fiz. Inst. Akad. Nauk USSR **5**, 339 (1950).
[10] P. A. Anfinrud and W. S. Struve, J. Phys. Chem. (in press).
[11] R. W. Chambers, T. Kajiwara, and D. R. Kearns, J. Phys. Chem. **78**, 380 (1981).
[12] C. R. Gochanour and M. D. Fayer, J. Phys. Chem. **85**, 1989 (1981).
[13] *Handbook for Chemistry and Physics*, edited by R. C. Weast (Chemical Rubber, Cleveland, 1975).
[14] M. Soltwisch and B. Steffen, Z. Naturforsch. Teil A **36**, 1045 (1981).
[15] D. W. Marquardt, Commun. ACM **13**, 47 (1970).
[16] T. J. Chuang and K. B. Eisenthal, J. Chem. Phys. **57**, 5094 (1972).
[17] A. Grinvald and I. Z. Steinberg, Anal. Biochem. **59**, 583 (1974).
[18] D. H. Waldeck and G. R. Fleming, J. Phys. Chem. **85**, 2614 (1981).
[19] W. L. Jorgensen, J. Am. Chem. Soc. **103**, 341 (1981).
[20] W. L. Jorgensen, J. Am. Chem. Soc. **103**, 345 (1981).
[21] D. L. Wertz and R. K. Kruh, J. Chem. Phys. **47**, 388 (1967).
[22] B. M. Pettitt and P. J. Rossky, J. Chem. Phys. **78**, 7296 (1983).
[23] H. van Koningsveld, Recl. Trav. Chim. Pays-Bas Belg. **87**, 243 (1968).
[24] O. Bastiansen, Acta Chem. Scand. **3**, 415 (1949).
[25] M. van Duin, J. M. A. Baas, and B. van de Graaf, J. Org. Chem. **51**, 1298 (1986).
[26] F. Podo, G. Nemethy, P. L. Indovina, L. Radics, and V. Viti, Mol. Phys. **27**, 521 (1974).
[27] A. E. Tenenbaum, L. M. Kaporovskii, and E. I. Shcherbina, Zh. Fiz. Khim. **52**, 1803 (1978).
[28] M. J. Sanders and M. J. Wirth, Chem. Phys. Lett. **101**, 361 (1983).
[29] *Crystal Data: Determinative Tables*, 3rd edition, edited by A. D. Mighell and J. K. Stalick (U. S. Dept. of Commerce, Washington 1983).
[30] R. S. Knox, Physica **39**, 361 (1968).